X-Band Dual Circularly Polarized Patch Antenna With High Gain for Small Satellites

Squadrito, Paolo; Zhang, Shuai; Pedersen, Gert Frølund

Published in:
IEEE Access

DOI (link to publication from Publisher):
10.1109/ACCESS.2019.2921088

Publication date:
2019

Document Version
Accepted author manuscript, peer reviewed version

X-Band Dual Circularly Polarized Patch Antenna with High Gain for Small Satellites

Paolo Squadrito, Shuai Zhang, *Senior Member, IEEE* and Gert Frølund Pedersen, *Senior Member, IEEE*

***Abstract*—This paper presents an X-band circularly polarized patch antenna with a simulated high gain of $12.5\,\mathrm{dBi}$ and a simulated side-lobe-level of below $-20\,\mathrm{dB}$, within the bandwidth of $5.2\,\%$. This single element antenna achieves high gain, by exploiting the mode superposition of $TM_{11} + TM_{13}$ (excited by a circle of vias loading the cavity) and $TM_{12} + TM_{14}$ (excited by the cavity itself) radiated from the two apertures, respectively. A simple feeding network, consisting of a quadrature hybrid and a couple of 90° bent branches, is used in the design to excite RHCP or LHCP modes in the antenna cavity. A capacitive disk feeding is implemented so that the antenna can be matched to the feeding network and the super-positioned fields inside the cavity are not disturbed by the feeding pins. This approach makes the design of a dual sense circularly polarized antenna with high gain easier since the array configuration is not needed. High gain, in combination with a dual-sense circular polarization, makes the proposed antenna particularly attractive for space applications involving small satellites. With the proposed design, it is possible to employ only one antenna rather than two (RHCP and LHCP), thus saving space on the aircraft, which is clearly a limited resource.**

***Index Terms*—circular patch, circular polarization, high gain, sidelobes suppression, small satellites.**

I. Introduction

THE access to the space segment is nowadays easier than ever, thanks to the recent advances done in miniaturization technology. As a matter of fact, the number of space mission involving small satellites in their different sizes is exponentially increasing [1]. Despite this recent growth, the concept of small satellite is not new. The relatively low cost of mass production and low launch cost are the main reason why small satellites are so attractive for small private companies or universities. In addition, the flexibility of this approach is another key aspect, which makes possible thanks to modern technologies, different kinds of missions like earth observation, remote sensing and of course communications. Although this comes with several challenges to face. Indeed the limited power on-board and the limited amount of area available are the main critical aspect of this kind of approach to space. The design of the antenna system is essential and different constraints must be taken into account from mission to mission.

For instance in [2], [3], transparent antennas are presented. This particular characteristic allows the allocation of the antenna on top of a solar panel, in order to save space on the platform. An S-band antenna system for earth observation is presented in [4]. This antenna shows a square window which is designed in order to accommodate the imaging system in the center. For downlink communications, deployable monopole or planar patch antennas working in UHF and S-band have been extensively employed, because of their lightweight and low-cost characteristics. For higher bit-rates, X-band is becoming more and more common [5] but, it is well-known that the aforementioned type of antennas in their classical configuration cannot provide the gain needed [6]. Increasing the aperture area of an antenna by employing an array configuration is a commonly used method to increase the gain. Besides the needs of relatively high gain, circularly polarized antennas are preferred since radio waves propagating through the ionosphere are subject to the Faraday Rotation Effect [7]. In [8]–[12] several circularly polarized arrays are presented. Often, both RHCP and LHCP polarizations are desired [13]–[16], which means that in some cases, two different antennas must be employed, so a doubled area is used. In [13], [14] dual circularly polarized dual band antennas are proposed. With this approach, however, only one polarization per band can be achieved. In [15] an aperture antenna is presented. Dual circular polarization is achieved, in this case, by using a new relatively complex feeding scheme for a four elements array. A low-profile circular patch antenna is presented in [17]. High gain and SLL suppression in a single element are the attractive characteristics of this antenna. On the other hand, this element is linearly polarized so it cannot be employed in several applications.

In this paper, a dual-sense circularly polarized planar antenna is presented. Following the same working principle exploited in [17], a high gain antenna with sidelobe suppression has been designed. Unlike the array configuration just mentioned, the proposed antenna is made by only one element which in turn allows a simple feeding network to be employed. By using a 90° hybrid, indeed, both RHCP and LHCP have been achieved in the same operative band. A capacitive feeding technique, in place of a traditional pin technique, has been employed in the proposed design. It is shown that by doing so, two main advantages are obtained. The first advantage in terms of impedance matching of the antenna to the feeding network. The second advantage in terms of purity of the fields inside the cavity, which are no longer disrupted by the feeding pin. This approach compared with the previously reported CP antennas bring several advantages, particularly for applications involving small satellites. On one hand, employing a single element makes the design of single

This work was supported by the InnovationsFonden project of MARS2.
Paolo Squadrito, Shuai Zhang, and Gert Frølund Pedersen are with the Antennas, Propagation and Millimeter-Wave Systems section at the Department of Electronic Systems, Aalborg University, Denmark
(email: pas,sz,gfp@es.aau.dk).
Corresponding author: Shuai Zhang.

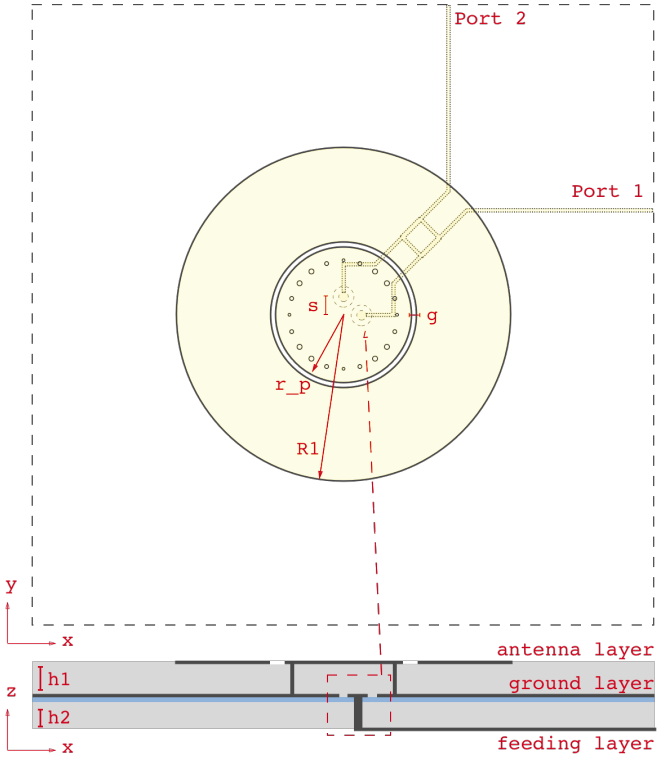

Fig. 1. Top view and side view of the proposed antenna layout. The metallizations are represented in black, the substrates (Roger 4350B) in grey and the glue film (Isola 370HR) in blue. Lines with the same dash step belong to the same layer.

band dual circularly polarized antennas easier since just a simple feeding network is needed. On the other hand the higher gain (compared with a conventional single element patch antenna) achieved by this design by exploiting the superposition of radiated fields, makes the antenna suitable to be employed in small satellites applications (for instance downlink communications). Thus avoiding dual band antennas like in [13], [14], or relatively complex feeding network like in [15]. This paper is organized as follows. Section II describes the antenna configurations. In this section, the challenges faced to design this kind of antenna and the proposed solution are presented. In section, III measured results and comparison are shown. Conclusion and possible future applications are discussed in section IV.

II. Antenna Configuration

A. Antenna and Feeding Network Design

In Fig.1 the configuration of the proposed antenna is shown. It has a 3 layers structure and the total dimension with regards to the wavelength is 3.7λ. The antenna layer is printed on a Roger 4350B with $\epsilon_r = 3.66$, $\tan\delta = 0.0037$ and thickness $h_1 = 1.524\,\mathrm{mm}$. It consist of a single circular element of radius $R1 = 27\,\mathrm{mm}$, with a circular slot of width $g = 0.8\,\mathrm{mm}$ etched at the position $r_p = 11.03\,\mathrm{mm}$. A circle of $N = 20$ grounded vias with non-identical diameter is placed at the position $r_c = 8.7\,\mathrm{mm}$. The diameters of the vias are $d_{small} = 0.6\,\mathrm{mm}$, $d_{medium} = 0.7\,\mathrm{mm}$ and $d_{large} = 0.8\,\mathrm{mm}$.

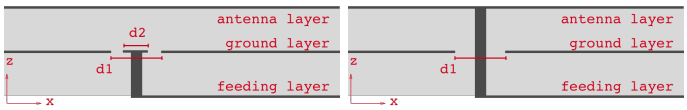

Fig. 2. Side view of the capacitive disk technique (a) made of a disk capacitively coupled with the antenna layer, and the pin technique (b) consisting of a pin going through the ground plane and connecting directly the antenna to the feeding network. For simplicity some details have been removed from this drawings.

With this choice the symmetry of the antenna in both E-plane and H-plane is preserved, thus allowing better performance in terms of polarization. The ground layer is printed on the other face of the Roger 4350B. Two circular apertures with diameter $d_1 = 3.4\,\mathrm{mm}$ (Fig.1 and Fig.2a) are etched in the ground plane at position $s = 3\,\mathrm{mm}$ along the x and y axes. A couple of metallic disks with diameter $d_2 = 1.6\,\mathrm{mm}$ are then placed in s and connected to the feeding network through a metallic pin. The feeding layer mainly consists of a quadrature hybrid connected to two $90°$ bent branches. This layer is printed on a Roger 4003C with $\epsilon_r = 3.55$, $\tan\delta = 0.0027$ and thickness $h_2 = 0.2\,\mathrm{mm}$ which in turn is glued to the ground layer through a thin film of Isola 370HR shown in blue in Fig.1.

B. Analysis of the Feeding Technique

A capacitive feeding technique has been chosen for the proposed antenna as shown in Fig.2a. As mentioned before the antenna cavity is fed through a couple of disks printed in the same layer of the ground plane. A common approach, among all, to achieve circular polarization is by exciting two orthogonal components with a $90°$ phase difference. The two disks are thus orthogonally placed and the $90°$ phase difference is provided by the quadrature hybrid. It is worthy to point out now that, by the nature of the quadrature hybrid, a dual-sense circularly polarized antenna is obtained. There are two main reasons for choosing a capacitive feeding technique over a traditional feeding with a pin going through a circular aperture in the ground plane and connecting the antenna directly to the feeding network as shown in Fig.2b. The first reason is related to the input impedance of the antenna. For a patch antenna operating with the fundamental mode, it is well known that the input impedance is maximum at the edge. This is no longer true when high order modes are excited in the cavity. In order to achieve high gain and improved SLL suppression, the proposed antenna exploit a superposition of radiated fields. A superposition of $TM_{11} + TM_{13}$ (radiating from the circular slot and from the outer aperture respectively) is excited at lower frequency by the circle of vias and a superposition of $TM_{12} + TM_{14}$ (radiating from the circular slot and from the outer aperture respectively) is excited at higher frequency by the cavity itself. In this case, the input impedance is maximum in a position between the center and the edge, depending on which high order mode is excited [18]. As a consequence of this, it is difficult to match the antenna to the feeding network. Fig.3 shows the real (a) and imaginary (b) part of the input impedance for both the techniques. The pin technique (solid

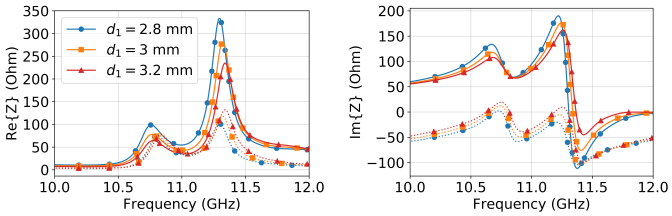

(a) (b)

Fig. 3. Simulated real (a) and imaginary (b) parts of the antenna input impedance for pin (solid line) and disk (dotted line) feeding technique.

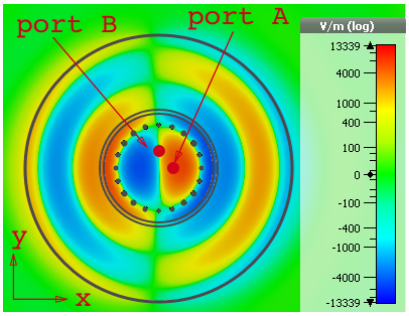

Fig. 4. Z component of the E-field excited in the cavity by only one port at 11 GHz. The edges of the metallic parts are represented in black and the feeding points are represented in red.

line) shows a higher resistance and reactance compared to the capacitive disk technique (dotted line). Moreover, the two degrees of freedom (the diameter of the circular aperture in the ground plane d_1 and the diameter of the circular disk d_2) given by this solution makes the impedance matching of the antenna easier. The second reason is related to the unwanted modes excited in the cavity. In a real scenario, the pin technique excites unwanted modes in the cavity [17]. This effect alters the purity of the TM_{1x} modes, which as said earlier, are exploited in the proposed design to achieve high gain and sidelobe level suppression. As said before, in applications where circular polarization is needed, a couple of pins are placed inside the cavity in orthogonal position in order to excite two orthogonal polarizations. When a pure TM_{1x} is excited this additional pin (which excite the orthogonal polarization) lies in a zero-field position. This is shown in Fig.4. The z components of the E-field inside the cavity excited by only port A at 11 GHz is represented. In this situation is clearly shown that port B is placed in a zero-fields area but when unwanted mode are excited this no longer applies. Therefore as a direct consequence, the two pins disrupt each other, narrowing down the radiation performance and deteriorating the isolation between the input port of the antenna. This effect can be mitigated by using a capacitive technique which is intrinsically free of metallic parts inside the antenna's cavity. It is worth to point out now, for a better understanding of the working principle of this antenna, that since only two modes are excited inside the cavity, only two resonances are shown in Fig.3. Consequently, each mode excited inside the cavity produces a superposition of radiated fields from the two apertures of the antenna.

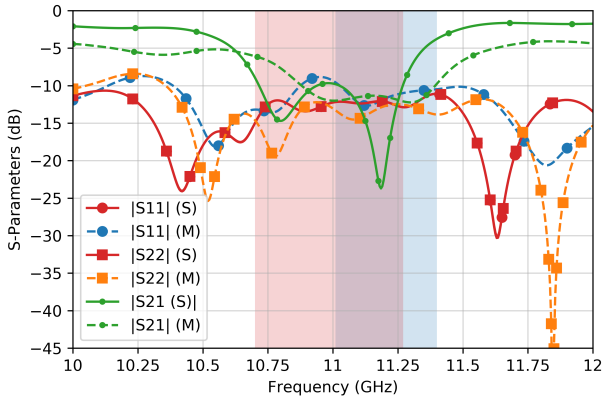

Fig. 5. Measured (M) and Simulated (S) $|S_{11}|$, $|S_{22}|$ and $|S_{21}|$. The impedance bandwidth of the manufactured antenna is highlighted in light blue. Simulated $|S_{22}|$ is not shown for reasons of symmetry.

III. Antenna Performance

According to what presented in section II a prototype of the proposed antenna has been realized and measured. The scattering parameters, measured with a Keysigth N5227A PNA, are shown in Fig.5. Both simulation and measurement show a wide range where the $|S_{xx}|$ is below $-10\,\mathrm{dB}$, with the exception of Port 1 for the manufactured antenna, which shows a small peak around 11 GHz. Taking into account S_{21}, the simulated antenna shows an impedance bandwidth of $5.2\,\%$ from $10.7\,\mathrm{GHz}$ to $11.27\,\mathrm{GHz}$ highlighted in red in Fig.5. The measured antenna shows an impedance bandwidth of $3.6\,\%$ from $11\,\mathrm{GHz}$ to $11.4\,\mathrm{GHz}$, highlighted in blue in Fig.5. Moreover, compared to the simulated results, the manufactured antenna band appears to be shifted to a slightly higher frequency. This discrepancy is related to a poor manufacture of the antenna which is relatively sensitive to the radius of the vias. This behavior has been observed in [17] already, so the results are not repeated in this work. The anechoic chamber shown in Fig.6 has been used to measure the radiation performances of the presented antenna. In this setup, the probe is placed on the yellow arm and the AUT is placed on the grey platform. By rotating the platform a full plane scanning is achieved. In order to measure both E-plane and H-plane, the AUT is thus manually rotated by $90°$. Gains and SLL are presented in Fig.7, once again the impedance bandwidth is highlighted in blue. The simulated gain is $13\,\mathrm{dBi}$. The measured gain is around $12.5\,\mathrm{dBi}$, which agrees with the simulated gain, with the only exception of a shift toward slightly higher frequency. On the other hand, simulation and measurement for the SLL seem to be rather different. The simulated SLL is around $-20\,\mathrm{dB}$, whereas the measured SLL is around $-10\,\mathrm{dB}$. However, the SLL shown by the manufactured antenna is quite similar to the one shown in [17] which is enough for the application. The simulated cross-polarization for both ports shows a cross-pol level around $-18\,\mathrm{dB}$ at $\theta = 0°$, the worst case is around $\theta = 45°$ where the cross-pol level is $0\,\mathrm{dB}$. Considering the relatively low level of the worst case and the fact that is outside the main beam

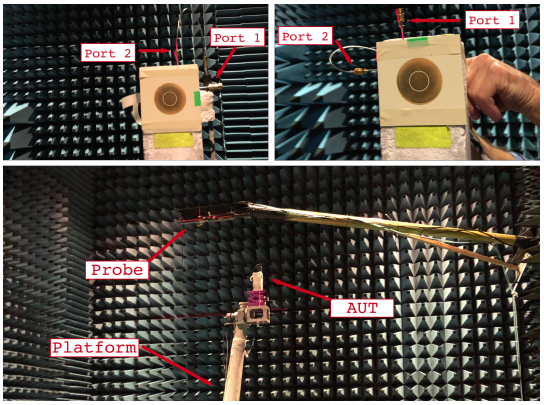

Fig. 6. Measurement setup employed for the proposed antenna. The probe is kept in a fixed position on the arm. The antenna under test is placed on the platform. Rotating the platform the E-plane or H-plane radiation pattern is measured.

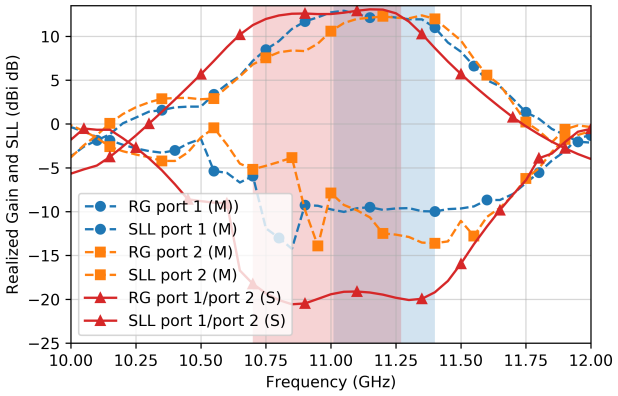

Fig. 7. Measured (M) and Simulated (S) Realized Gain (RG) and Side Lobe Level (SLL) for port 1 and port 2. The impedance bandwidth of the manufactured antenna is highlighted in light blue. For reason of symmetry the simulated results for port 2 are omitted.

area, the results are omitted. Results for the axial ratio are presented in Fig.8. The simulated results show an $AR < 3\,\mathrm{dB}$ in a large band. The in-band axial ratio level for port 1 is a bit high because of a peak around 11 GHz. On the other hand, measured results for port 2 show better performance with an $AR < 2\,\mathrm{dB}$ in the whole impedance bandwidth. Due to the symmetry of the structure, the AR for the two ports should be the same thus the differences are due to imperfection in the manufacturing process. Fig.9 shows the realized gain of the manufactured antenna for both ports in the two main planes compared with the simulated results. The simulated results are shown in the band from 10.75 GHz to 11.25 GHz and the measured results are shown in the band 11 GHz to 11.4 GHz due to the small shift to a higher frequency. The first sidelobe seems to appear around $\pm 50°$ for the measurement and around $\pm 110°$ for the simulations, which could explain the difference between the curves in Fig.7.

IV. Conclusion

In this paper, an X-band circular polarized patch antenna. Simulations have shown a high gain of 12.5 dBi and a SLL

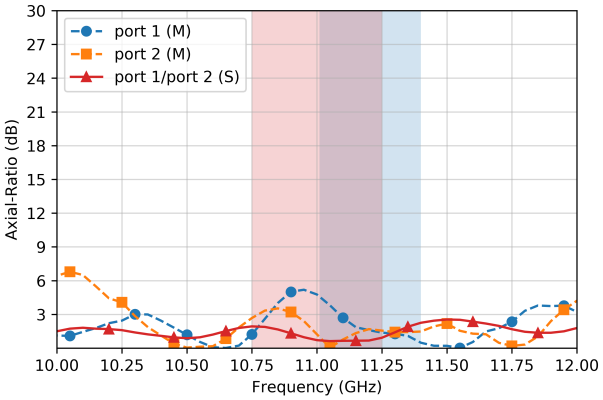

Fig. 8. Measured (M) and Simulated (S) Axial Ratio for port 1 and port 2. The impedance bandwidth of the manufactured antenna is highlighted in light blue.

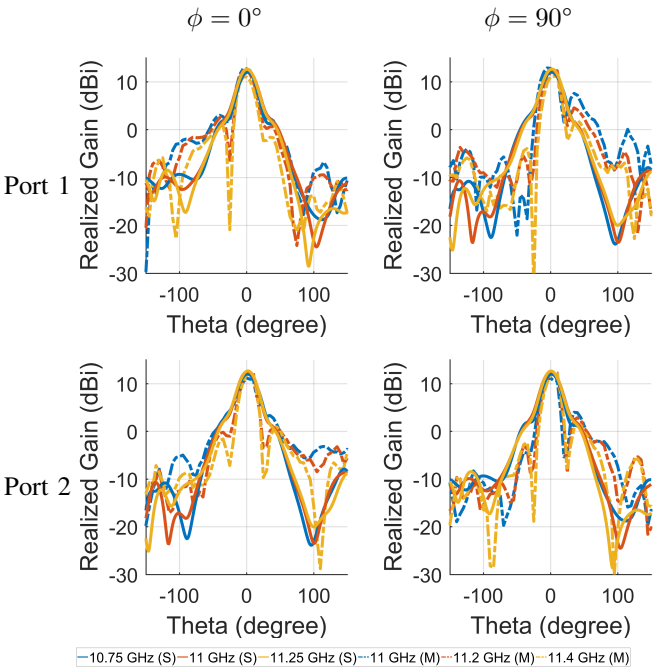

Fig. 9. Measured (M) and Simulated (S) radiation patterns for E-plane and H-plane at three different frequency points. Results are shown for port 1 and port 2.

better than $-20\,\mathrm{dB}$, in a bandwidth of 5.2 %. For this single element antenna, the high gain has been achieved, by exploiting a superposition of fields radiated from two apertures. A simple feeding network consisting of a quadrature hybrid and a couple of 90° bent branches have been used in the proposed design, in order to excite RHCP or LHCP modes in the antenna cavity. This approach makes the design of a dual sense circularly polarized antenna with high gain easier since the array configuration or other more complex solution are not needed. Because of the advantages in terms of impedance matching and modes purity, a capacitive feeding technique, rather than a pin feeding technique, has been chosen to feed the antenna. High gain, in combination with a dual-sense circular polarization, make the proposed antenna particularly

attractive for space applications involving small satellites. For instance, the proposed antenna could be employed for downlink applications where, to the best knowledge of the authors, two separate antennas arrays operating in the same band (one for the RHCP and another one for LHCP) are used. Consequently, space, which is clearly a very limited resource on a small satellite, is saved. It is worth to point out that, for practical reason, a high dielectric constant has been chosen for the manufacturing of this antenna. This choice limits the gain that otherwise would be up to $16\,\mathrm{dBi}$ [17] which is considered enough for downlink applications in low earth orbit.

REFERENCES

[1] (2018) Nanosatellite launches since 1998. [Online]. Available: https://www.nanosats.eu/img/fig/Nanosats_years_black_2018-10-28.png

[2] X. Liu, J. Liu, D. R. Jackson, J. Chen, P. W. Fink, and G. Y. Lin, "Broadband transparent circularly-polarized microstrip antennas for cubesats," in *2016 IEEE International Symposium on Antennas and Propagation (APSURSI)*, June 2016, pp. 1545–1546.

[3] J. Sun and K. Luk, "A wideband low cost and optically transparent water patch antenna with omnidirectional conical beam radiation patterns," *IEEE Transactions on Antennas and Propagation*, vol. 65, no. 9, pp. 4478–4485, Sept 2017.

[4] A. Nascetti, E. Pittella, P. Teofilatto, and S. Pisa, "High-gain s-band patch antenna system for earth-observation cubesat satellites," *IEEE Antennas and Wireless Propagation Letters*, vol. 14, pp. 434–437, 2015.

[5] (2018) Nanosatellite downlink frequencies and bands. [Online]. Available: https://www.nanosats.eu/img/fig/Nanosats_frequency_black_2018-10-28.png

[6] C. A. Balanis, *Antenna theory: analysis and design*. Wiley-Interscience, 2005.

[7] E. Sorensen, "Magneto-ionic faraday rotation of the radio signals on 40 mc from satellite 1957 (sputnik i)," *IRE Transactions on Antennas and Propagation*, vol. 9, no. 3, pp. 241–247, May 1961.

[8] S. Lin and Y. Lin, "A compact sequential-phase feed using uniform transmission lines for circularly polarized sequential-rotation arrays," *IEEE Transactions on Antennas and Propagation*, vol. 59, no. 7, pp. 2721–2724, July 2011.

[9] A. Chen, Y. Zhang, Z. Chen, and C. Yang, "Development of aka-band wideband circularly polarized 64-element microstrip antenna array with double application of the sequential rotation feeding technique," *IEEE Antennas and Wireless Propagation Letters*, vol. 10, pp. 1270–1273, 2011.

[10] C. Deng, Y. Li, Z. Zhang, and Z. Feng, "A wideband sequential-phase fed circularly polarized patch array," *IEEE Transactions on Antennas and Propagation*, vol. 62, no. 7, pp. 3890–3893, July 2014.

[11] S. Mohammadi-Asl, J. Nourinia, C. Ghobadi, and M. Majidzadeh, "Wideband compact circularly polarized sequentially rotated array antenna with sequential-phase feed network," *IEEE Antennas and Wireless Propagation Letters*, vol. 16, pp. 3176–3179, 2017.

[12] K. Ding, C. Gao, D. Qu, and Q. Yin, "Compact broadband circularly polarized antenna with parasitic patches," *IEEE Transactions on Antennas and Propagation*, vol. 65, no. 9, pp. 4854–4857, Sept 2017.

[13] J. Zhang, W. Wu, and D. Fang, "Dual-band and dual-circularly polarized shared-aperture array antennas with single-layer substrate," *IEEE Transactions on Antennas and Propagation*, vol. 64, no. 1, pp. 109–116, Jan 2016.

[14] T. Yue, Z. H. Jiang, and D. H. Werner, "A compact metasurface-enabled dual-band dual-circularly polarized antenna loaded with complementary split ring resonators," *IEEE Transactions on Antennas and Propagation*, vol. 67, no. 2, pp. 794–803, Feb 2019.

[15] J. Zhu, S. Liao, Y. Yang, S. Li, and Q. Xue, "60 ghz dual-circularly polarized planar aperture antenna and array," *IEEE Transactions on Antennas and Propagation*, vol. 66, no. 2, pp. 1014–1019, Feb 2018.

[16] Q. Wu, J. Hirokawa, J. Yin, C. Yu, H. Wang, and W. Hong, "Millimeter-wave multibeam endfire dual-circularly polarized antenna array for 5g wireless applications," *IEEE Transactions on Antennas and Propagation*, vol. 66, no. 9, pp. 4930–4935, Sep. 2018.

[17] P. Squadrito, S. Zhang, and G. F. Pedersen, "Wideband or dual-band low-profile circular patch antenna with high-gain and sidelobe suppression," *IEEE Transactions on Antennas and Propagation*, vol. 66, no. 6, pp. 3166–3171, June 2018.

[18] P. Juyal and L. Shafai, "A novel high-gain printed antenna configuration based onTm_{12}mode of circular disc," *IEEE Transactions on Antennas and Propagation*, vol. 64, no. 2, pp. 790–796, Feb 2016.